STANFORD RESEARCH INSTITUTE
MENLO PARK, CALIFORNIA

June 1964

Final Report

THE EFFECTS OF A PLASMA IN THE NEAR-ZONE FIELD OF AN ANTENNA

Prepared for:

NATIONAL AERONAUTICS AND SPACE ADMINISTRATION
LANGLEY RESEARCH CENTER
HAMPTON, VIRGINIA

CONTRACT NAS1-3099

By: W. C. TAYLOR D. E. WEISSMAN

SRI Project 4555

Approved: T. MORITA, MANAGER
ELECTROMAGNETIC SCIENCES LABORATORY

D. R. SCHEUCH, DIRECTOR
ELECTRONICS AND RADIO SCIENCES DIVISION

Copy No. 1

ABSTRACT

The report studies the problem of radiating energy from an antenna immersed in a finite plasma, under various conditions of the ratios of the collision frequency and the plasma frequency to the Radian Frequency. This has been done by focusing attention on the two basic types of radiators—the small dipole and loop—and observing their properties, theoretically and experimentally, in a dissipative medium similar to that present on a re-entry vehicle. Consideration has also been given to the impedance-matching problem with small antennas, and also to the effects of sheaths surrounding the antenna surface.

CONTENTS

ILLUSTRATIONS

I INTRODUCTION

The attenuation of electromagnetic waves propagating through a plasma has been the subject of considerable attention in recent years: However, when an antenna is immersed in a plasma, there are more than merely propagation losses. The ability of the antenna to radiate RF energy to great distances is affected by the proximity of the plasma in several ways. In the usual terminology, two important effects are:

(1) The dissipation due to immersion of near-fields in a conducting medium, acting as a shunt conductance to which a large share of the power may be directed; and

(2) The altered ability of the antenna to radiate when surrounded by a reactive or dissipative medium.

These two effects concern the division of the available power between radiating and dissipating modes. However, since the impedance is changed by the presence of the plasma, the power delivered to the antenna will also be changed from the free-space value, and this third effect must be accounted for in an over-all consideration of "plasma losses" in the usual insertion-loss meaning of the term. Still a fourth effect is due to the space-charge sheath that forms around bodies immersed in a plasma due to the difference in mobility between electrons and ions. A fifth problem (especially associated with near-field plasmas) is the reduced threshold for nonlinear effects similar to breakdown experienced when a plasma covers the antenna aperture.

Thus it is seen that, pattern considerations aside, the total power radiated may be diminished due to at least five effects in addition to ordinary wave attenuation. Although the last two named occur in plasma more often than in other dissipative media, they are nevertheless less general in plasmas than the first three effects. The emphasis of the first year's effort on this contract has been upon these first three effects. Section II of this report summarizes the analysis of (1) and (2) above as they apply to small loops and dipoles immersed in plasmas of infinite extent. With such a model, the distinction is made very clearly between these near-field effects and propagation losses. As a combined measure of these two effects, a radiation efficiency in plasma

is both defined and derived for these two antennas, demonstrating their behavior as plasma conditions are varied widely.

Section III reports the program of measurements with a small dipole and a small loop in a seeded hydrocarbon flame. Results are presented showing the VSWR and the loss of radiated power, and comparisons are made with the theory developed in Sec. II.

Section IV is a discussion of the application of the elementary concepts developed for loops and dipoles to more commonly used re-entry antenna systems. An outgrowth of this discussion are recommendations for future measurements.

II ANALYSIS OF LOOP AND DIPOLE RADIATION EFFICIENCY IN PLASMA

The dependence of fields upon distance from an electrically small dipole or loop, immersed in an infinite plasma with phase and attenuation constants β and α, will be of the form $(e^{-\alpha r}/r^m)$, where m is an integer. In a plasma, as opposed to the free-space case, the fields with $m > 1$ carry real power away from the antenna to the medium. However, beyond a sphere of radius equal to λ_p, the wavelength in the plasma, the only important fields are those with $m = 1$. This means the total power flux through any such surface $r \geq \lambda_p$ can be written as

$$W_r \approx \frac{|I|^2}{2} R_p e^{-2\alpha r} \qquad r \geq \lambda_p \tag{1}$$

where I is the current at the antenna terminals. It is shown in Appendix B that, by integrating the expressions for the fields, R_p is given by

$$\begin{cases} \dfrac{\beta}{\beta_0} R_d & \text{for dipole} \\ \dfrac{\beta(\beta^2 + \alpha^2)}{\beta_0^3} R_l & \text{for loop,} \end{cases} \tag{2}$$

where R_d and R_l are the free-space radiation resistances of the dipole and loop, respectively.

If Eq. (1) is rearranged in the form

$$W_r e^{2\alpha r} \approx \frac{|I|^2}{2} R_p = W_p \qquad r \geq \lambda_p, \tag{3}$$

Eq. (3) suggests that R_p can be considered a radiation resistance representing not W_r, evaluated at some $r \geq \lambda_p$, but W_p, which is merely

W_r referenced at $r = 0$ by assuming an $(e^{-\alpha r}/r)$ dependence of the "propagating fields" within λ_p. The convenience of this definition will immediately be shown.

Then a figure of merit that is independent of r and unique to a given antenna in a given plasma can be defined as η_p, the antenna plasma radiation efficiency given by

$$\eta_p = \frac{W_p}{W_T} = \frac{R_p}{\mathrm{Re}(Z_p)} \qquad r \geq \lambda_p \tag{4}$$

where W_T is the total power delivered to the antenna and Z_p is the complex antenna impedance measured at its terminals. Thus, to find the over-all radiation efficiency including propagation losses at a given distance, r, η_p is multiplied by $e^{-2\alpha r}$.

The scaling procedure suggested by Deschamps[1*] is used for calculating $\mathrm{Re}(Z_p)$ from free-space models of the antenna impedance. If the total impedance of an antenna in free space is given by

$$Z(\omega, \epsilon_0) = R(\omega, \epsilon_0) + jX(\omega, \epsilon_0) \quad , \tag{5}$$

where ϵ_0 is the free-space dielectric constant, then the impedance in plasma described by complex index of refraction n becomes

$$Z_p = \frac{Z(n\omega, \epsilon_0)}{n} = \frac{R(n\omega, \epsilon_0)}{n} + j\,\frac{X(n\omega, \epsilon_0)}{n} \quad . \tag{6}$$

Because n is complex, each of the functions $R(n\omega, \epsilon_0)$ and $X(n\omega, \epsilon_0)$ will, in general, give rise to both real and imaginary terms. Because for small loops and dipoles, $X(\omega, \epsilon_0) >> R(\omega, \epsilon_0)$, the imaginary terms from $[X(n\omega, \epsilon_0)/n]$ comprise the important part of $\mathrm{Re}(Z_p)$ for plasma densities of interest.

For the dipole, approximations from Ref. 2 give†

$$\mathrm{Re}(Z_p) \approx \left[\frac{2\alpha}{\beta} + \frac{\beta^3 h^3}{3(\Omega - 3)}\right] X_d(\omega, \epsilon_0) \cdot \left(\frac{\beta_0}{\beta}\right)^2 \tag{7}$$

---

* References are listed at the end of the report.

† See Appendix C

where $\Omega = 2\ ln\ (2h/a)$ and the dimensions h and a are illustrated in the sketch accompanying Fig. 1. The first term in the brackets in Eq. (7) is the important loss term, arising from the free-space capacitive reactance.

For the loop, however, the usual free-space inductance term gives no real contribution in plasma, and second-order terms must be used. From Chen and King[3], it can be shown that, for $\beta b \gtrsim 0.3$, where b is the loop diameter,

$$Z(\omega, \epsilon_0) \approx \left[X_l \frac{\beta_0^3 b^3}{6C_1} + j\ (1 + C_2 \beta_0^2 h^2) \right] \tag{8}$$

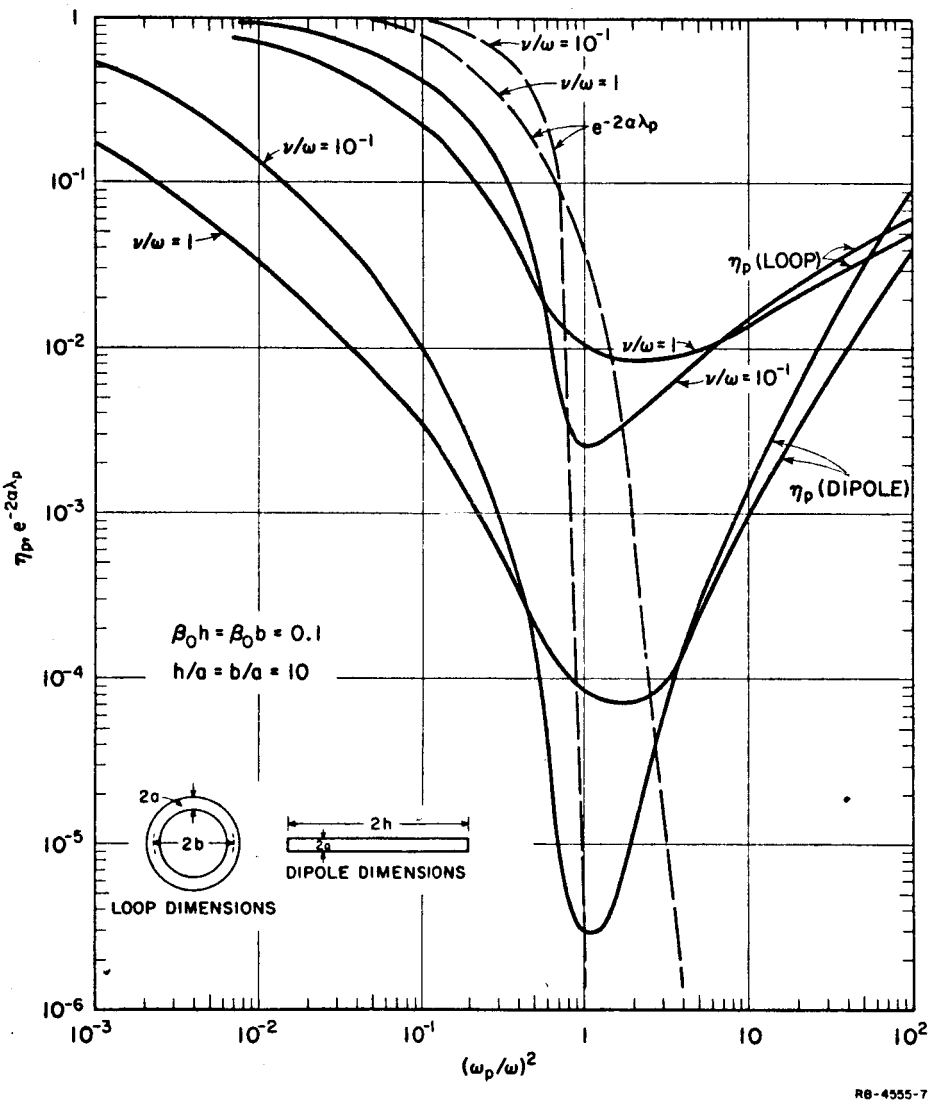

FIG. 1 RADIATION EFFICIENCY, η_p, AND PROPAGATION LOSSES, $e^{-2\alpha\lambda_p}$, FOR ONE WAVELENGTH SPHERE AS A FUNCTION OF NORMALIZED PLASMA FREQUENCY

where X_l is the free-space loop inductive reactance, $C_1 = (1/\pi)[ln(8b/a)-2]$ and $C = 2+(2/3\pi C_1)$. In a plasma, Eq. (8) gives

$$\mathrm{Re}\,(Z_p) = X_l \left[2C_2 b^2 \alpha\beta + \frac{b^3}{6C_1}(\beta^3 - 3\alpha^2\beta)\right] \qquad (9)$$

Again the most important loss term, the first in Eq. (9), arises from a free-space reactance term.

Then from Eqs. (2), (7) and (9), we get

$$\eta_p = \frac{(\beta/\beta_0)^3}{\left[\frac{2\alpha}{\beta} + \frac{\beta^3 h^3}{3(\Omega - 3)}\right]} \frac{R_d}{X_d(\omega, \epsilon_0)} \qquad \text{for dipole}$$

$$= \frac{\beta^3 h^3/3(\Omega - 3)}{\left[\frac{2\alpha}{\beta} + \frac{\beta^3 h^3}{3(\Omega - 3)}\right]} \qquad (10)$$

and

$$\eta_p = \frac{1}{\left[2C_2 b^2 \alpha\beta + \frac{b^3}{6C_1}(\beta^3 - 3\alpha^2\beta)\right]} \frac{R_l}{X_l} \qquad \text{for loop}$$

$$= \frac{\beta_0^3\, b^3/6C_1}{\left[2C_2 b^2 \alpha\beta + \frac{b^3}{6C_1}(\beta^3 - 3\alpha^2\beta)\right]} \qquad (11)$$

Equations (10) and (11) are plotted in Fig. 1 as a function of the plasma frequency, ω_p, normalized by ω, for different values of normalized collision frequency, ν/ω, with dimensions as noted on the figure. These plots show clearly a "resonance" behavior of near-field losses in small loops and dipoles as represented by the radiation efficiency when plotted

over a large range of the normalized plasma frequency. Since it appears from the character of these curves that all plasma losses might decrease for ω_p/ω greater than 10^2, it should be noted that the over-all radiation efficiency, including propagation losses, at a distance r is $\eta_p e^{-2\alpha r}$, where α is an increasingly large number as ω_p/ω exceeds unity, and the analysis applies only for $r > \lambda_p$. Thus the quantity $e^{-2\alpha\lambda_p}$ has also been plotted on the same coordinates in Fig. 1 for the same values of collision frequency to allow comparison with η_p. This plot shows that the near-field losses are more important than the propagation losses for $(\omega_p/\omega) \gtrsim 1$.

The collision frequency is seen to be an important parameter in the radiation efficiency function. The curves of Fig. 1 show that lowering the collision frequency with a given antenna, improves the radiation efficiency for almost all values of the plasma frequency. The exception is when the plasma frequency is in a small range about the RF frequency. In this range, the deepest nulls of η_p occur for the lower values of (ν/ω). The minima of η_p are shifted to the right by increased (ν/ω). This marked resonance behavior of η_p is unique to those media, such as plasma, in which α can exceed β and which approach a completely cut-off condition as (ν/ω) approaches zero. The effect of increased collision frequency on the over-all radiation efficiency, $\eta_p e^{-2\alpha r}$, is seen to vary, depending upon the range of $(\omega_p/\omega)^2$ and the value of r of interest.

An important factor that the curves do not show is the effect of changing h and b. Since the fractions R/X in Eqs. (10) and (11) represent the reciprocal of the free-space Q of the respective antennas, and vary as $(\beta_0 h)^3$ and $(\beta_0 b)^3$, respectively, it is seen that, for high α, η_p for the dipole varies as $(\beta_0 h)^3$, but for the loop only as $(\beta_0 b)$. Hence if $\beta_0 h = \beta_0 b = 0.3$ (the maximum values for which the theory is valid), the Q of each antenna compared with those illustrated in the figure is decreased by a factor of 27. Hence the minimum value of the dipole η_p is increased compared with the figure by a factor of 27 and the loop η_p minimum by a factor of only three.

It is noted from the right side of the figure that in plasmas similar to sea water ($\alpha^2 >> \beta_0^2$ and $\beta^2 >> \beta_0^2$), the radiation efficiency alone gives little to choose from between small loops and small dipoles.

III EXPERIMENTAL PROGRAM

A. OBJECTIVES

Since the theory of antennas in conductive media is simplest for very small antennas, these were chosen for the first experimental effort so comparisons could readily be made with theory. It was decided to construct a small dipole and a small loop by mounting a stub and a half loop over a ground plane, since this would allow them to be connected to a coaxial line on which impedance and power could be measured conveniently (see Figs. 2 and 3).

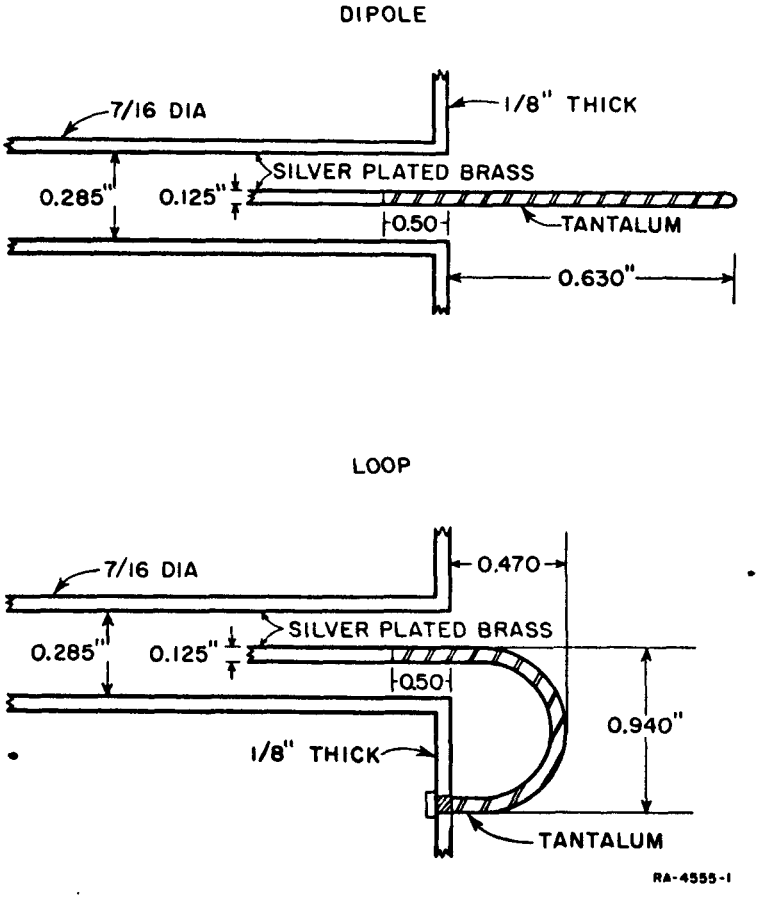

FIG. 2 HALF DIPOLE AND LOOP CONSTRUCTED FOR FLAME MEASUREMENTS

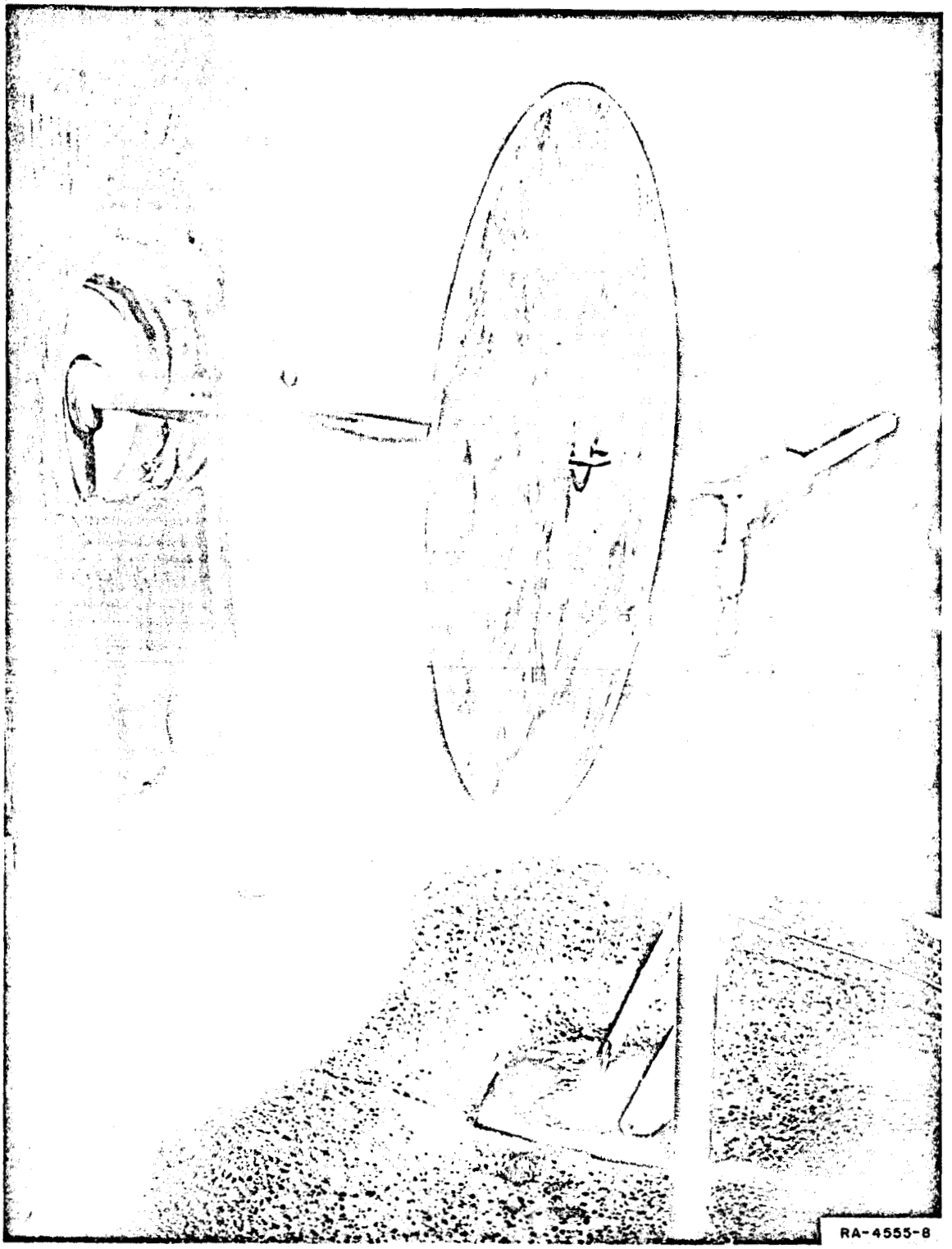

FIG. 3 LOOP ANTENNA IN MEASUREMENT LOCATION

From Sec. II it is seen that the total power radiated beyond a sphere of radius r equals the product of the power delivered to the antenna terminals, the radiation efficiency, and the exponential factor $e^{-2\alpha r}$, provided r exceeds one wavelength in the plasma. The radiation efficiency was defined in an infinite, homogeneous medium and it can be a useful parameter in the following way: If two different antennas (for instance, a dipole and loop) draw the same amount of power from a generator, then the ratio of the powers that each will transmit beyond a sphere of a given radius will be the ratio of their radiation efficiencies, and this ratio will not depend on the radius provided $r \geq \lambda_p$. If the medium outside this sphere should be replaced by free space, then the ratio of the respective powers radiated beyond the sphere for the given antennas will also be the ratio of their radiation efficiencies. This is because the patterns for very small antennas have approximately the same form, even in the conducting medium, and the wave impedances are the same, so that the reflection coefficient from the interface will be the same for both antennas. It is this property of the ratio of the radiation efficiencies that the experiments with a finite, flame-produced, plasma tried to observe. The ratio of the dipole radiation efficiency to that of the loop can be greater or less than unity, depending on their relative sizes and on the parameters of the medium. For the size antennas that were designed for our experiments, and the constants of the hydrocarbon flame, the calculations for an infinite, homogeneous medium showed the loop to be superior to the dipole throughout the range calculated.

Thus it was the purpose of the experiments to measure two quantities which can be compared with the theory of Sec. II. One is the VSWR of the antennas in flame, and the other is the ratio of radiation efficiencies.

B. EXPERIMENTAL SETUP

The experimental apparatus can be separated into two main groups. The first group is comprised of the low-pressure vessel in which the flame is burned, the associated gas metering equipment, the vacuum system and the flame diagnostic equipment. The details of this group are described in Appendix A. The second group contains the RF equipment used to measure impedance, radiated and received power, and the test antennas. A schematic of this latter setup is shown in Fig. 4.

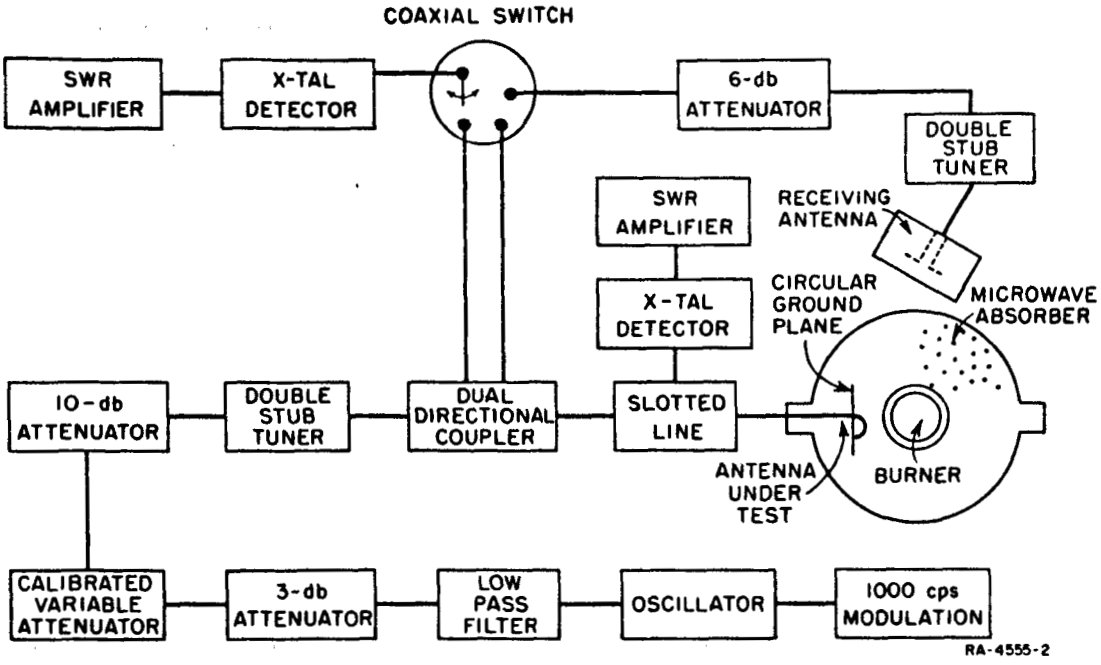

FIG. 4 SCHEMATIC OF SETUP FOR IMPEDANCE AND RADIATION MEASUREMENTS

The test antennas (Fig. 2) were the termination of a rigid, silver plated brass, coaxial transmission line. The transmission line was supported by a vacuum seal, mounted on a side arm of the vessel, which permitted it to move the antenna in and out of the flame. The antenna was positioned 10 inches above the burner (see Fig. 3). The antenna could be left in the flame only a few minutes, during which time the electron density and electrical measurements were made.

The electron density of the flame was enhanced by placing a crucible containing NaCl on the edge of the burner opening and allowing the salt to evaporate and ionize the flame. Some typical profiles are plotted in Fig. 5. The range of electron density that was attainable was from one-fourth to three times the critical value, measured at the tip of the antenna. The critical electron density is the density at which the plasma frequency equals the RF frequency.

All of the measurements were taken at a single pressure so the collision frequency remained constant and estimated at 1.6 times the radian RF frequency. Since the flame has a large percentage of water vapor, the collision frequency is largely determined by collisions between electrons and water molecules, since at these flame temperatures (1000°K) the collision cross section for water is larger than the other combustion

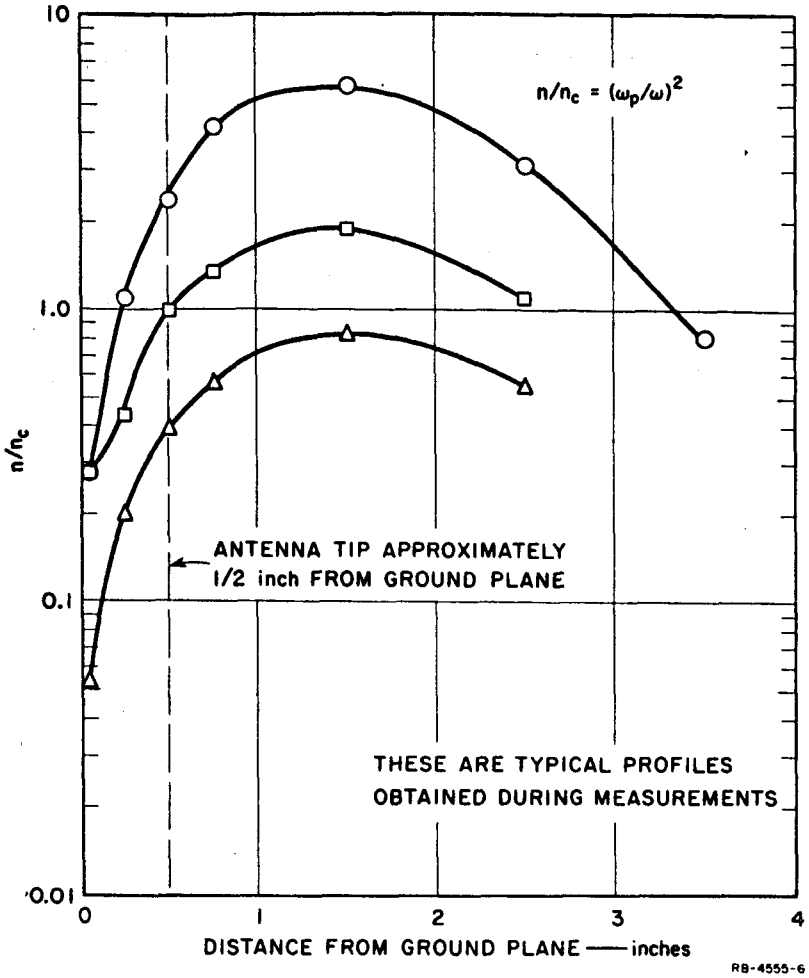

FIG. 5 ELECTRON DENSITY RELATIVE TO THE CRITICAL VALUE vs. DISTANCE FROM GROUND PLANE

products. The collision frequency for this flame has been measured as a function of pressure and the results are available in Ref. 4.

The receiving antenna was positioned 30 degrees from the ground plane, outside the glass vessel. This choice of position was determined only by the fixed arrangement of the chamber apparatus. Since it is assumed that the far field pattern of each antenna is unchanged by the flame, it is considered that the receiving antenna receives a constant fraction of the power radiated beyond the plasma under all conditions. This assumption will be discussed further in the next section.

C. DATA

Before the flame was ignited, each antenna was mounted in its test position over the burner, and the VSWR and voltage minimum position measured.

Also measured was the level of P_{inc}, the power incident on the antenna terminals, and the level of P_{rec}, the power received by the receiving antenna. The power delivered to the antenna, P_{del}, was calculated by standard transmission line theory from P_{inc} and the VSWR.

It is assumed that the receiving antenna received a constant fraction F of P_{del} such that

$$\left(\frac{P_{rec}}{P_{del}}\right)_{free\text{-}space} = F \quad .$$

The above procedure is repeated under various flame conditions, in which case

$$\left(\frac{P_{rec}}{P_{del}}\right)_{flame} = F\eta e^{-2\alpha r} \quad .$$

Combining these equations, we get

$$\left(\frac{P_{rec}}{P_{del}}\right)_{flame} = \left(\frac{P_{rec}}{P_{del}}\right)_{free\text{-}space} \eta e^{-2\alpha r} \quad ,$$

or

$$R = \eta e^{-2\alpha r} \quad ,$$

where

$$R = \left(\frac{P_{rec}}{P_{del}}\right)_{flame} \Big/ \left(\frac{P_{rec}}{P_{del}}\right)_{free\text{-}space} \quad .$$

The measured ratio R is plotted for the loop and for the dipole in Fig. 6. The ratio of R for the loop to R for the dipole in the same flame will give the ratio of their radiation efficiencies. This can be compared to the theoretical result (Fig. 7) where the radiation efficiencies in an infinite medium are plotted. The ratio of radiation efficiencies is shown by the dotted line.

Since the plasma about each antenna was inhomogeneous, having a minimum at the ground plane and a maximum approximately one inch beyond the tip

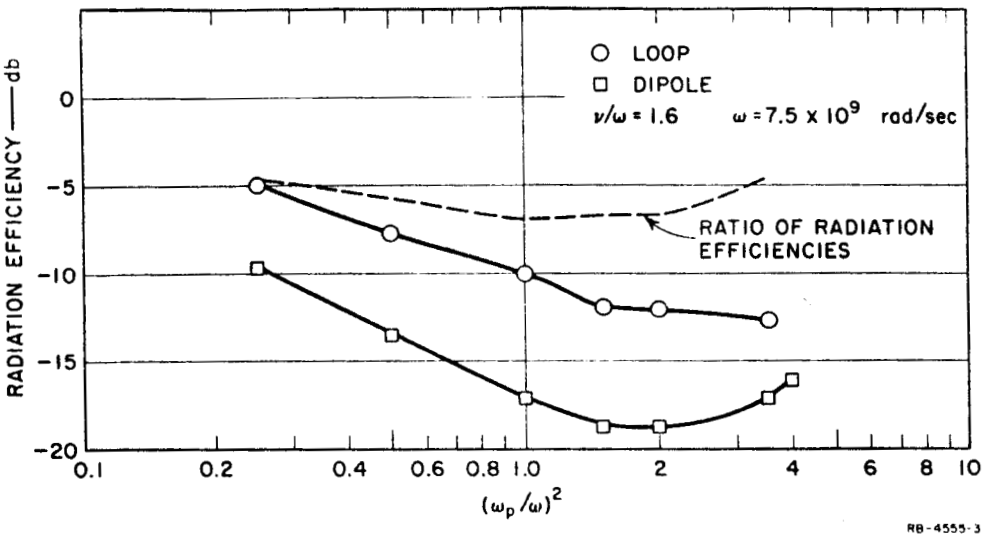

FIG. 7 CALCULATED RADIATION FREQUENCY FOR DIPOLE AND LOOP IN INFINITE, HOMOGENEOUS PLASMA vs. NORMALIZED PLASMA FREQUENCY

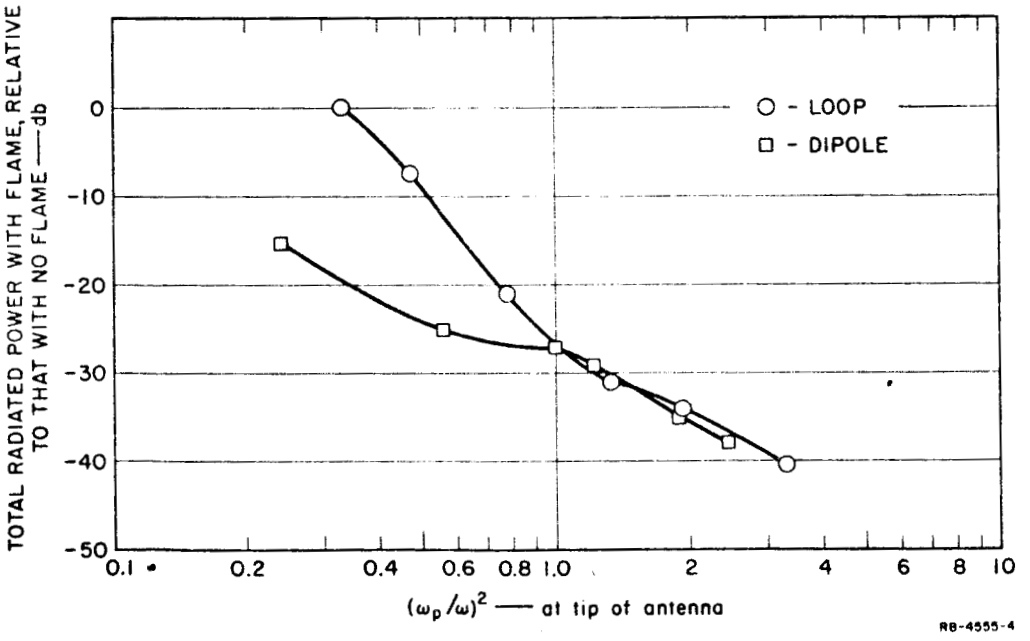

FIG. 6 DROP IN TOTAL RADIATED POWER DUE TO FLAME vs. NORMALIZED PLASMA FREQUENCY

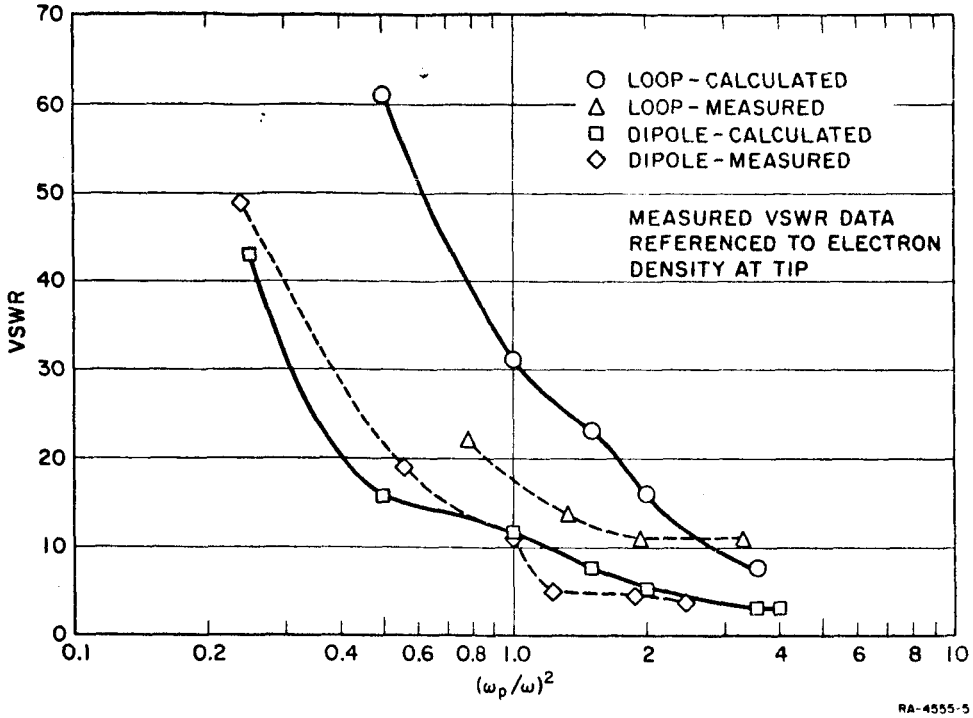

FIG. 8 CALCULATED AND MEASURED VSWR OF DIPOLE AND LOOP vs. NORMALIZED PLASMA FREQUENCY

(Fig. 8), the density at the tip was arbitrarily chosen as the abscissa against which the VSWR and other data were plotted. No such ambiguity exists for the theoretical VSWR since the medium is assumed homogeneous. These curves of the VSWR are shown in Fig. 8.

D. DISCUSSION OF EXPERIMENTAL RESULTS

The VSWR data for both of the antennas was in reasonable agreement with the theory, considering the inhomogeneity of the plasma. This data substantiates the theory that near field losses will be largest for those antennas that store more electric energy in their near fields.

The data that was taken to compare with the theoretical radiation efficiencies was interpreted under the assumption that the far field patterns of the antennas will not be affected by the flame. While this assumption is all right for electron densities under critical, it is felt that it becomes poorer as the electron density increases beyond its critical value, because of the two dimensional inhomogeneity of the electron density. Below the critical density, however, the data does show, qualitatively, the superiority of the loop in radiating power.

For these data, also, the abscissa of the graphs is the electron density at the tip of the antenna. Because of this ambiguity it will not be fruitful to quantitatively compare the theoretical curves of radiation efficiency with this data, since they were calculated under firm restrictions on the size, symmetry and uniformity of the plasma.

Another feature of this data is the merging of the curves in Fig. (6) at the higher electron densities. This suggests the increasing dominance of the exponential attenuation, at these densities, over the near field effects, which are more noticeable at the lower densities. Under these higher density conditions the dipole and loop, which are comparable size, are very similar in performance.

IV NEAR-FIELD EFFECTS IN PRACTICAL ANTENNA SYSTEMS

A. GENERAL

The understanding of the loop and dipole behavior in plasmas under the simple conditions of complete immersion in plasmas of infinite extent is important to understanding more specialized classes of problems such as large antennas with near fields only partially immersed in plasmas of finite extent. In addition, the prior sections of this report have not treated some of the effects that are appropriate to both the loop and dipole as well as larger antennas. This section gives a discussion of both of these classes of problems as they are expected to influence communication and diagnostic equipment on a reentry vehicle.

B. FEED GAP LOSSES IN PLASMA

The impedance calculated in Sec. II of this report assumes an infinitesimal gap at the feed points. The losses in a gap of finite size that is exposed to plasma may be significant. In air, this feed effect is usually represented by a shunt reactance across the antenna. In a lossy plasma, the gap will act like a capacitor filled with a lossy dielectric and will add conductance and susceptance to the antenna admittance. This will represent energy stored and dissipated in the nonradiating electric fields in the feed region. For a given feed geometry, the effect of this shunt impedance on the power delivered to the radiating structure will depend on the impedance of the radiating structure. An antenna that has an admittance comparable to the gap admittance (for instance a small dipole) will allow the gap to shunt a substantial portion of the available power.

C. IMPEDANCE-MATCHING CONSIDERATIONS

The case where no matching network is placed between an antenna and a generator will first be considered. The effect of a transmission line joining the two will be of interest. The generator impedance will be assumed resistive and equal to Z_0, the transmission line characteristic impedance. Then the effects of a matching network will be considered.

If an antenna is connected to a generator through a lossless transmission line ($\alpha_{Line} = 0$), all the power delivered to the input of the transmission line will be absorbed in the antenna, regardless of the VSWR on the transmission line. For the realistic case where the transmission line has some finite loss, it is possible that more power will be dissipated in the transmission line than will be delivered to the antenna impedance. The higher the VSWR of the antenna impedance, the poorer will be the efficiency. For the case where $\alpha l \ll 1$ neper, and $S > 20$,

$$\frac{\text{Power delivered to antenna impedance}}{\text{Power delivered to input of transmission line}} = \frac{\frac{1}{S}}{\alpha l + \frac{1}{S}}$$

The term S is the VSWR of the antenna that would be observed on a lossless transmission line of the same Z_0. A reduction of S results in less reflected power at the transmission line input plus an increase in the efficiency of the network, both of which result in greater power to the antenna. Therefore, if a high-Q antenna were immersed in a thin plasma, part of the losses due to near-field dissipation in the plasma would be compensated by increased power to the antenna in this circuit since the VSWR would be lowered by these losses.

In place of the direct single transmission line connection to the transmitter, a matching network—possibly consisting of lumped reactive elements and sections of transmission lines—will next be considered. For a high-Q antenna, the circuit which matches it, in air, to a resistive generator impedance will also cause a severe mismatch when the antenna is immersed in a plasma that causes its impedance to change appreciably. For lossless matching elements, the VSWR on the generator side of the matching network determines the power delivered to the antenna. If there are losses in the matching elements, it is possible that the power division between the radiation resistances of a short antenna and the equivalent loss resistance of the matching elements will be poor in air but will improve under plasma conditions. Losses in the matching elements could also prevent small changes in the resistive part of the antenna impedance from disturbing the impedance match appreciably (if $Q_{ant} \gg Q_{ckt}$) while the power delivered to the antenna increases because of the lowered S and hence more favorable power division.

Therefore, it is desirable to use an antenna with as low a Q as possible to minimize the mismatch caused by the matching circuit in the plasma regime. The Q of the matching circuit will only be important in free space, when it will be less than the antenna Q, and will limit the efficiency of the network.

D. SHEATH EFFECT FOR SMALL DIPOLE AND LOOP

One of the features that distinguish a plasma from an ordinary conductive medium—such as sea water—is that the negative charge carriers are free electrons, not negative ions, and they have a much greater mobility than the lightest positive ion. An object that is placed inside a neutral plasma will initially receive a larger random electron current than ion current and will accumulate a negative charge on its surface, which will repel other electrons from the immediate vicinity of the surface. The electrostatic potential produced by this accumulating surface charge will increase until both electron and ion currents to the surface are equal, making the net current zero. Also, between this surface charge on the object and the plasma, a sheath occupied by ions will be formed. This sheath will be found in any plasma, *i.e.*, for any value of ν/ω_p, and will be of the order of several Debye lengths thick.[5]

If a voltage is applied to either the dipole or loop whose $\omega >> \omega_p$, the electrons outside the sheath will not be able to respond to this varying voltage and the total charge on the antenna and total charge of the ions in the sheath will not vary. The effect on the propagating fields is that the antenna appears to be surrounded by a lossless dielectric with a dielectric constant approximately equal to ϵ_0, of extent corresponding to the sheath boundaries. The dielectric outside this region has the usual plasma properties. Therefore, the plasma will have a negligible effect on the antenna impedance as well as on the propagation.

For frequencies lower than ω_p, the sheath dimensions will respond to the RF frequency. The result is a varying sheath capacitance and an increase in the antenna conductance. Therefore, in this plasma regime, where propagation is cutoff or attenuated, the presence of the sheath will be seen in the antenna impedance and any effort to diagnose the plasma from antenna impedance measurements should include a knowledge of the sheath dimensions and sheath motion. These parameters will depend on the relative magnitudes of the antenna radius, Debye length, the mean free path, and the values of ν/ω.

V SUMMARY AND CONCLUSIONS

The subject of antennas in lossy media adds another degree of freedom to an already broad topic. The object of this study has been to focus attention on the two basic types of radiators and to compare their properties in a dissipative medium similar to that present on a re-entry vehicle. The experimental results are in good agreement with the linear theory for these antennas.

Besides the direct experiments made, study of the theoretical impedance and radiation properties of these antennas has yielded information about some practical problems, such as the effects of antenna Q on impedance matching, the effect of the feed point on the antenna impedance and some other features of the impedance matching problem that are faced when an antenna must radiate both in and out of a plasma.

The studies reported above suggest several other possible topics for study. One is the effect of an irregular, small plasma on the far field patterns of the elemental antennas. Another topic would be the study of larger dipoles and loops, those that are naturally efficient radiators, and to note the effect of the plasma on these antennas. The slot antenna would also be included in this group.

APPENDIX A

EXPERIMENTAL APPARATUS

APPENDIX A

EXPERIMENTAL APPARATUS

1. LOW-PRESSURE FLAME EQUIPMENT

The low-pressure chamber was a 20-inch cylindrical section of pyrex glass. Two 4-inch-diameter ports were added on opposite sides to provide flat glass viewing areas for the optical temperature measurement. All access to the chamber for gas lines, water lines, and Langmuir probe was through the base plate. The steel plate which formed the top of the chamber, as well as a short section of the 4-inch exhaust line above it, were water-cooled. A water-cooled baffle section to further cool the gas was inserted in the exhaust line before the 4-inch gate valve used for flow control. The vacuum pump, which is located outside the building, is a 200-cfm rotary gas ballast pump. The gas ballast feature of the pump system is necessary because large amounts of water vapor must be handled.

A premixed ethylene-oxygen flame was used in the experiment.

$$C_2H_4 + 3O_2 \rightarrow 2H_2O + 2CO_2 + \text{Heat}$$

The CO_2 and H_2O subsequently disassociate into CO, H_2, O_2, OH, O and H. These disassociations, which are endothermic, use an enormous amount of heat, which limits the flame temperature. The ethylene gas was used because of its relatively high temperature--about 2500 degrees K—and ease of handling. Nitrogen (N_2) is also used occasionally as a diluent; the nitrogen provides some measure of control of flow rate as well as flame speed, and thus of flame position relative to the burner. The gas equipment is depicted in Fig. A-1. The gas flow to the burner is controlled by a nullmatic pressure regulator and jeweled metering orifice. The gas flow through the critical orifice is directly proportional to the orifice area and gas supply pressure.

$$v = kk'Ap$$

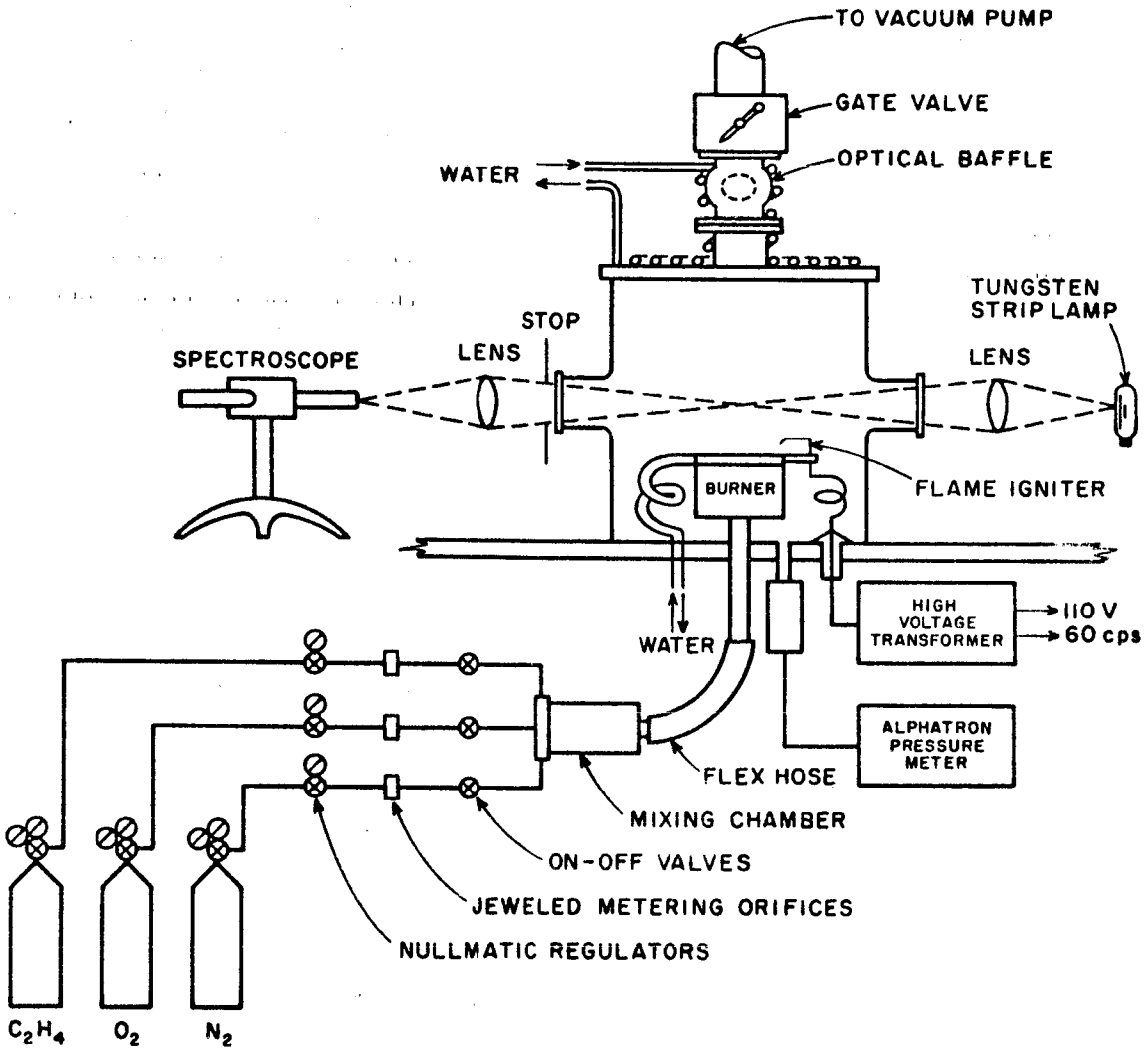

FIG. A-1 LOW-PRESSURE FLAME APPARATUS

where

v = flow through critical flow orifice
k = includes the gas constants and temperature
k' = orifice efficiency
A = orifice cross sectional area
p = upstream pressure.

In order to obtain the proportional flow condition it is necessary that the sonic flow be obtained in the orifice throat. This requirement is met when the pressure ratio (upstream pressure/downstream pressure) across the orifice is about 3:1 or greater. In this experiment the pressure ratio was on the order of 100.

After the various gases are metered they pass to a mixing chamber, which serves also to prevent flow resonances. The premixed gas is then passed to the burner through a flexible hose so that the burner can be raised and lowered while the flame is burning. The burner consists of six aluminum rings 1/2inch high by 3 inches OD by 2 inches ID, between each of which is inserted a fine mesh stainless steel screen to diffuse the gases so that at the burner top a uniform velocity exists across the burner surface. The top screen, which is water cooled around the edge, is a perforated 20-gauge stainless steel sheet with 1/8 inch holes

The gas mixture was ignited by a glow discharge formed about an electrode adjacent to the burner. The high voltage was supplied from a 60-cycle high-voltage transformer.

The pressure within the system was measured by an Alphatron ionization gauge. The gauge was checked periodically against a differential manometer.

Flames were sustained within the chamber over the 1 to 40 mm Hg pressure range. At the high and low ends of this range some restrictions were encountered in mixture ratios and flow rates. Over a substantial portion of the pressure range, however, a reasonably wide range of mixture ratios and flow rates could be accommodated.

2. TEMPERATURE MEASUREMENT

The temperature of the gases above the flame was measured using the sodium line reversal technique. When sodium is introduced into a flame the yellow sodium D lines (5890 and 5896 Å) are emitted. It can be shown from Kirchhoff's law that when light from a bright background source, such as a tungsten strip lamp, giving a continuous spectrum, is passed through a flame containing sodium vapor, the sodium lines will appear either in absorption, as dark lines against the continuum, or as bright lines, standing out brighter than the continuum, according to whether the brightness temperature of the background source is higher or lower than the flame temperature. When the brightness of the two sources is the same the temperatures are the same. By measuring the temperature of the tungsten filament with an optical pyrometer, and assuming that the sodium is the equilibrium temperature of the gas, the gas temperature is known. The sodium, in the form of salt (NaCl), was introduced into the flame for two reasons: to measure temperature and to enhance the electron density by the easily ionized sodium (Na).

3. ELECTROSTATIC PROBE FOR ELECTRON DENSITY MEASUREMENT

The electrostatic probe is a conductor immersed in a plasma to which a voltage is applied. The variation of the current drawn by the probe as the voltage is varied produces a curve which has the characteristic shape shown in Fig. A-2.

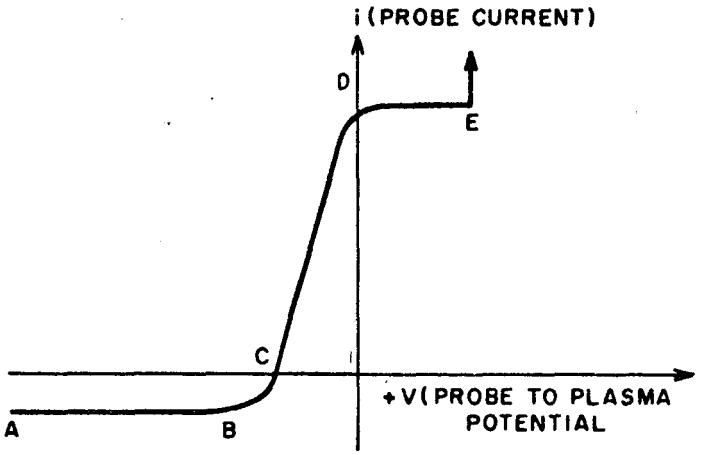

FIG. A-2 TYPICAL PLOT OF CURRENT AS A FUNCTION OF VOLTAGE FOR AN ELECTROSTATIC PROBE

When the probe is highly negative (*AB* in Fig. A-2) with respect to the plasma, positive ions are attracted to the probe and electrons are repelled. Thus the current collected is predominantly made up of positive ions. Because of the preponderance of positive ions and the lack of electrons near the probe, a positive space charge is developed in that region which limits the current collected by the probe. The probe and plasma form a system similar to a diode; the plasma acts as the cathode and the probe acts as the anode.

As the probe is made less highly negative (*BC* in Fig. A-2), a point is reached at which a few high-energy electrons are able to reach the probe. The current is then made up of electrons and positive ions so that the measured current is

$$i_m = i_+ + i_e \quad .$$

Since the electron current is made up of charges of opposite sign from the positive-ion current, the measured current decreases.

The positive ion current through the probe when negatively biased has been related to the ion density (hence electron density) in the plasma by several authors.[6,7,8] Chen's analysis,[7] assuming as usual that the probe radius is much larger than several Debye lengths and that the probe radius is small compared with mean-free path, gives the simple approximate result

$$i_+ = KAn_0e(2kT_E/M)^{1/2}$$

where K is a constant, of the order of unity, which depends on the probe geometry and also slightly on the ion temperature. Reference 7 gives $K \approx 0.4$.

This method of measuring the electron density, while requiring an independent measurement or estimate of the electron temperature, was not expected to be influenced as much by the depletion of the charges in the vicinity of the probe since the level of current is down approximately two orders of magnitude from the readings needed to establish the actual density on the electron side of the curve.

APPENDIX B

TOTAL POWER RADIATED BY A DIPOLE AND LOOP IN AN INFINITE CONDUCTING MEDIUM

APPENDIX. B

TOTAL POWER RADIATED BY A DIPOLE AND LOOP IN AN INFINITE CONDUCTING MEDIUM

The total average power radiated beyond a sphere of radius r, is

$$W_r = \text{Real Part} \left\{ \int_0^{2\pi} d\phi \int_0^{\pi} S_r(r) r^2 \sin\theta d\theta \right\}$$

Complex Poynting Vector

$$\vec{S}(r) = \frac{1}{2} E \times \vec{H}^* \quad ,$$

where

$$\vec{E} = E_r \vec{a}_r + E_\theta \vec{a}_\theta + E_\phi \vec{a}_\phi \quad ,$$

$$\vec{H} = H_r \vec{a}_r + H_\theta \vec{a}_\theta + H_\phi \vec{a}_\phi \quad , \quad \text{and}$$

* denotes complex conjugate .

The $\vec{a}$'s are the unit vectors in the spherical coordinate system. The components of the field vectors and phasors, with $e^{j\omega t}$ suppressed. The coordinate θ will denote angles with respect to the axis of the electric or magnetic dipole moment.

For the dipole: (Triangular current distribution, half height h)

$$E_\theta \doteq \frac{j\omega\mu_0 I(0)h}{4\pi} \left(\frac{k}{r} - \frac{j}{r^2} - \frac{1}{kr^3} \right) e^{-jkr} \sin\theta$$

$$E_r \doteq \frac{\omega\mu_0 I(0)h}{4\pi k} \left(\frac{2}{r^2} - \frac{2j}{kr^3} \right) e^{-jkr} \cos\theta$$

$$H_\phi \doteq \frac{j\mu_0 I(0)h}{4\pi} \left(\frac{k}{r} - \frac{j}{r^2} \right) e^{-jkr} \sin\theta$$

for $r > h$

$I(0)$ denotes the current at the feed point

$$k^2 = \omega^2 \mu_0 \epsilon \quad ,$$

where k is the complex wave number, and ϵ is the complex dielectric constant.

For a plasma

$$\frac{\epsilon}{\epsilon_0} = 1 - \frac{\left(\frac{\omega_p}{\omega}\right)^2}{1 + \left(\frac{\nu}{\omega}\right)^2} - j \frac{\left(\frac{\nu}{\omega}\right)\left(\frac{\omega_p}{\omega}\right)^2}{1 + \left(\frac{\nu}{\omega}\right)^2}$$

ν = collision frequency

ω_p = plasma frequency.

Also

$k = \beta - j\alpha$ $\qquad$ β = phase constant

$= \omega \sqrt{\mu_0 \epsilon}$ $\qquad$ α = attenuation constant

$= \beta_0 \sqrt{\frac{\epsilon}{\epsilon_0}}$

Making this substitution for k,

$$\text{Re}\ [S_r(r)] = \text{Re}\left\{\frac{1}{2} E_\theta H_\phi^*\right\} = \frac{|I(0)|^2 \omega \mu_0 \beta h^2}{32\pi r^2}\left(1 + \frac{\alpha}{\beta} L\right) e^{-2\alpha r} \sin^2 \theta$$

where

$$L = \frac{2}{\left(1 + \frac{\alpha^2}{\beta^2}\right)\beta r} + \frac{4\alpha\beta}{\left(1 + \frac{\alpha^2}{\beta^2}\right)\beta^2 r^2} + \frac{2}{\left(1 + \frac{\alpha^2}{\beta^2}\right)\beta^3 r^3} \quad .$$

For r chosen sufficiently large to make $\beta r >> 1$, and if $\alpha \leq \beta$, then $L << 1$

$$W_r = \frac{|I(0)|^2}{2}\left(\frac{\beta h^2 \omega \mu_0}{6\pi}\right) e^{-2\alpha r} \quad .$$

Since

$$\frac{\omega\mu_0}{\beta_0} = \sqrt{\frac{\mu_0}{\epsilon_0}} = 120\pi \quad ,$$

$$W_r = \frac{|I(0)|^2}{2} (20\beta_0 \cdot \beta \cdot h^2) e^{-2\alpha r} \quad .$$

Radiation resistance in free space $= 20\beta_0^2 h^2 \triangleq R_d$

$$W_r = \frac{|I(0)|^2}{2} \left(\frac{\beta}{\beta_0} R_d\right) e^{-2\alpha r} \quad .$$

For the loop = (uniform current, radius b)

$$E_\phi = \frac{\omega\mu}{4\pi}\left(\frac{k}{r} - \frac{j}{r^2}\right) |m| \sin\theta \, e^{-jkr}$$

$$H_r = \frac{1}{4\pi}\left(\frac{2}{r^3} + j\frac{2k}{r^2}\right) |m| \cos\theta \, e^{-jkr}$$

$$H_\theta = \frac{1}{4\pi}\left(\frac{1}{r^3} + j\frac{k}{r^2} - \frac{k^2}{r}\right) |m| \sin\theta \, e^{-jkr}$$

m = magnetic dipole moment $= \pi b^2 I(0)$.

Again substituting $k = \beta - j\alpha$

$$\text{Re}\{S_r(r)\} = \frac{1}{2} \text{Re}[-E_\phi H_\theta^*]$$

$$= \frac{\omega\mu|m|^2}{32\pi^2} \frac{\beta(\beta^2+\alpha^2)}{r^2} \left[1 + \frac{2\alpha}{(\beta^2+\alpha^2)}\right] e^{-2\alpha r} \sin^2\theta$$

$$= \frac{\omega\mu|I(0)|^2 b^4}{32} \frac{\beta(\beta^2+\alpha^2)}{r^2} \left[1 + \frac{2\alpha}{(\beta^2+\alpha^2)}\right] e^{-2\alpha r} \sin^2\theta \quad .$$

After integration over a sphere, on which $\beta r >> 1$

$$W_r = \frac{|I(0)|^2}{2} \frac{\beta(\beta^2 + \alpha^2)}{\beta_0^3} R_l e^{-2\alpha r}$$

R_l = free space radiation resistance = $20\pi^2(\beta_0 b)^4$.

APPENDIX C

IMPEDANCE OF A SMALL DIPOLE IN AN UNBOUNDED PLASMA OF MODERATE CONDUCTIVITY

APPENDIX C

IMPEDANCE OF A SMALL DIPOLE IN AN UNBOUNDED PLASMA OF MODERATE CONDUCTIVITY

In a plasma for which $(2\alpha/\beta)^2 \ll 1$, the admittance of a small dipole ($\beta h \leq 0.3$) has been shown to be[2]

$$Y_p = G + jB = \frac{2\pi}{\zeta_e \psi_{d1}} \left\{ \frac{2\alpha}{\beta} \left[\beta h + \frac{2}{3} \beta^3 h^3 F \right] + \frac{\beta^3 h^3}{3(\Omega - 3)} + j \left[\beta h + \frac{1}{3} \beta^3 h^3 F - \frac{5}{3} \frac{\alpha}{\beta} \frac{\beta^4 h^4}{(\Omega - 3)} \right] \right\} ,$$

where

$$\zeta_e = \omega \mu_0 / \beta$$

$$\psi_{d1} = 2 \ln (h/a) - 2 \qquad \Omega = 2 \ln (2h/a)$$

$$F = 1 + [(3 \ln 2 - 1)/(\Omega - 3)]$$

$$\mathrm{Re}\{Z_p\} = \mathrm{Re}\left\{\frac{1}{Y_p}\right\} = \frac{G}{G^2 + B^2}$$

$$\doteq \left[2 \frac{\alpha}{\beta} \left(1 + \frac{2}{3} \beta^2 h^2 F \right) + \frac{\beta^3 h^3}{3(\Omega - 3)} \right] \left(\frac{\zeta_e \psi_{d1}}{2\pi \beta h} \right)$$

The radiation efficiency is then

$$\eta_p \text{ (dipole)} = \frac{\frac{\beta}{\beta_0} R_d}{\mathrm{Re}\{Z_p\}} = \frac{\frac{\beta}{\beta_0} R_d}{\left[\frac{2\alpha}{\beta} + \frac{\beta^3 h^3}{3(\Omega - 3)} \right] \left(\frac{\beta_0}{\beta} \right)^2 X_d} ,$$

where R_d and X_d are the free space radiation resistance and reactance, respectively.

$$\eta_p \text{ (dipole)} = \frac{\left(\frac{\beta}{\beta_0}\right)^3 R_d}{\left[\frac{2\alpha}{\beta} + \frac{\beta^3 h^3}{3(\Omega - 3)}\right] X_d}$$

APPENDIX D

IMPEDANCE OF A SMALL LOOP IN AN UNBOUNDED PLASMA OF MODERATE CONDUCTIVITY

APPENDIX D

IMPEDANCE OF A SMALL LOOP IN AN UNBOUNDED PLASMA OF MODERATE CONDUCTIVITY

For a small loop, namely $\beta b \leq 0.3$, King and Chen[3] have shown that

$$Y_p \doteq -j \frac{1}{120\pi^2(\beta_0 b)} \left[1 - 2(kb)^2\right] \frac{1}{K_1} .$$

$k = \beta - j\alpha$

b = loop radius

a = wire radius

$$K_1 \doteq \frac{1}{\pi} ln \frac{8b}{a} - \frac{1}{\pi}\left[2 - \frac{2}{3}(kb)^2\right] - j\left[\frac{1}{6}(kb)^3\right] \quad \text{and} \quad \alpha \leq \beta$$

$$Z_p \doteq j(120\pi^2\beta_0 b) \frac{K_1}{[1 - 2(kb)^2]} .$$

Separating real and imaginary parts,

$$\text{Re}\{Z_p\} = (120\pi\beta_0 b)\left[\left(ln \frac{8b}{a}\right) - 2\right]\left[2(\alpha b)(\beta b)\left\{2 + \frac{2}{3\left[\left(ln \frac{8b}{a}\right) - 2\right]}\right\} + \frac{(\beta b)\pi[(\beta b)^2 - (\alpha b)^2]}{6\left(ln \frac{8b}{a}\right) - 2}\right] .$$

$$\text{Re}\ \{Z_p\} = X_l \left[4(\alpha b)(\beta b) \left(1 + \frac{1}{3\left[\left(ln\ \frac{8b}{a} - 6\right]\right.} \right) + \frac{\pi\beta b[(\beta b)^2 - (\alpha b)^2]}{6\left[\left(ln\ \frac{8b}{a}\right) - 2\right]} \right]$$

where X_l is the free space reactance, and is

$$= (120\pi\beta_0 b)\left[\left(ln\ \frac{8b}{a}\right) - 2\right] .$$

The radiation efficiency for the loop is then

$$\eta_p\ (\text{Loop}) = \frac{\frac{\beta(\beta^2 + \alpha^2)}{\beta_0^3} R_l}{\text{Re}\ [Z_p]}$$

$$\eta_p = \frac{\frac{\beta(\beta^2 + \alpha^2)}{\beta_0^3} R_l}{X_l \left\{ 4(\alpha b)(\beta b) \left(1 + \frac{1}{3\left[\left(ln\ \frac{8b}{a}\right) - 6\right]} \right) + \frac{\pi\beta b[(\beta b)^2 - (\alpha b)^2]}{6\left[\left(ln\ \frac{8b}{a}\right) - 12\right]} \right\}}$$

REFERENCES

1. Deschamps, G. A. "Impedance of an Antenna in a Conducting Medium," *Trans IRE*, AP-10, p. 648, (September 1962).

2. King, R. W. P., C. W. Harrison, and D. H. Denton, "The Electrically Short Antenna as a Probe for Measuring Free Electron Density and Collision Frequencies in an Ionized Region," *J. Research Natl. Bur. Standards, Sec. D*, 65, p. 371, (July-August 1961).

3. Chen, C. L., and R. W. P. King, "Small Bare Loop Antenna Immersed in Dissipative Medium," *Trans. IEEE*, AP-11, pp. 266-269, (May 1963).

4. Chown, J. B., "A Study of Plasma Induced Voltage Breakdown at Low Pressure," Final Report, Purchase Order 2-009203-9155 under Contract AF 33(600)-41517 with Boeing Airplane Company, SRI Project 3369, Stanford Research Institute, Menlo Park, California, (July 1961).

5. Rose, D. J., and M. Clark Jr., *Plasma and Controlled Fusion*, (John Wiley and Sons, Inc., New York, N.Y., 1964).

6. Allen, J. F., R. L. F. Boyd, and P. Reynolds, "The Collection of Positive Ions by a Probe Immersed in a Plasma," *Proc. Phys. Soc. (London), Sec. B*, 70, pp. 297-304, (March 1, 1957).

7. Chen, F. F., "Use of Electrostatic Probes in Plasma Physics," Proc. Joint Nuclear Instrumentation Symposium, *IRE Trans.*NS-8, pp. 150-154, (October 1961).

8. Wharton, C. B., "A Survey of Plasma Instrumentation " Proc. Joint Nuclear Instrumentation Symposium, *IRE Trans.* NS-8, pp. 56-70, (October 1961).

STANFORD RESEARCH INSTITUTE

MENLO PARK
CALIFORNIA

Regional Offices and Laboratories

Southern California Laboratories
820 Mission Street
South Pasadena, California 91031

Washington Office
808–17th Street, N.W.
Washington, D.C. 20006

New York Office
270 Park Avenue, Room 1770
New York, New York 10017

Detroit Office
1025 East Maple Road
Birmingham, Michigan 48011

European Office
Pelikanstrasse 37
Zurich 1, Switzerland

Japan Office
Nomura Security Building, 6th Floor
1–1 Nihonbashidori, Chuo-ku
Tokyo, Japan

Retained Representatives

Toronto, Ontario, Canada
Cyril A. Ing
67 Yonge Street, Room 710
Toronto 1, Ontario, Canada

Milan, Italy
Lorenzo Franceschini
Via Macedonio Melloni, 49
Milan, Italy